Clin Neuroradiol (2019) 29:645–651
https://doi.org/10.1007/s00062-018-0722-0

ORIGINAL ARTICLE

MDCT-based Finite Element Analysis of Vertebral Fracture Risk: What Dose is Needed?

D. Anitha[1] · Kai Mei[2] · Michael Dieckmeyer[2] · Felix K. Kopp[2] · Nico Sollmann[3] · Claus Zimmer[3] · Jan S. Kirschke[3] · Peter B. Noel[2] · Thomas Baum[3] · Karupppasamy Subburaj[1]

Received: 21 May 2018 / Accepted: 3 August 2018 / Published online: 21 August 2018

Abstract

Purpose The aim of this study was to compare vertebral failure loads, predicted from finite element (FE) analysis of patients with and without osteoporotic vertebral fractures (OVF) at virtually reduced dose levels, compared to standard-dose exposure from multidetector computed tomography (MDCT) imaging and evaluate whether ultra-low dose derived FE analysis can still differentiate patient groups.

Materials and Methods An institutional review board (IRB) approval was obtained for this retrospective study. A total of 16 patients were evaluated at standard-dose MDCT; eight with and eight without OVF. Images were reconstructed at virtually reduced dose levels (i.e. half, quarter and tenth of the standard dose). Failure load was determined at L1–3 from FE analysis and compared between standard, half, quarter, and tenth doses and used to differentiate between fracture and control groups.

Results Failure load derived at standard dose (3254 ± 909 N and 3794 ± 984 N) did not significantly differ from half (3390 ± 890 N and 3860 ± 1063 N) and quarter dose (3375 ± 915 N and 3925 ± 990 N) but was significantly higher for one tenth dose (4513 ± 1762 N and 4766 ± 1628 N) for fracture and control groups, respectively. Failure load differed significantly between the two groups at standard, half and quarter doses, but not at tenth dose. Receiver operating characteristic (ROC) curve analysis also demonstrated that standard, half, and quarter doses can significantly differentiate the fracture from the control group.

Conclusion The use of MDCT enables a dose reduction of at least 75% compared to standard-dose for an adequate prediction of vertebral failure load based on non-invasive FE analysis.

Keywords Multidetector computed tomography · Radiation dosage · Spinal fractures · Finite element analysis · Osteoporosis

Introduction

Osteoporosis is a skeletal disorder characterized by compromised bone strength. Osteoporotic fractures are usually caused by low-energy mechanisms and are frequently not apparent at the spine until symptomatic back pain presents [1]. Thus, initiation of therapy in patients with prevalent osteoporotic vertebral fractures is often delayed.

Dual-energy X-ray absorptiometry (DXA)-based areal bone mineral density (BMD) overlaps between patients with and without osteoporotic fractures [2]. Volumetric BMD assessed by multi-detector computed tomography (MDCT) can be used as a surrogate marker for fracture risk. Wang et al. [3] reported that finite element (FE) modelling and volumetric BMD consistently improved vertebral fracture risk assessment compared to areal BMD by DXA; however, Kopperdahl et al. observed incident radiographically confirmed spinal fractures to be associated with FE modelling independent of vertebral volumetric BMD [4]. Thus, BMD is limited in predicting bone strength, since it does not consider bone geometry, and the bone density distribution. The MDCT-based FE analysis enables an excellent prediction of osteoporotic vertebral fracture

✉ Karupppasamy Subburaj
subburaj@sutd.edu.sg

1 Engineering Product Development (EPD) Pillar, Singapore University of Technology and Design (SUTD), 8 Somapah Road, 487372 Singapore, Singapore

2 Department of Radiology, Klinikum rechts der Isar, Technical University of Munich, Munich, Germany

3 Department of Neuroradiology, Klinikum rechts der Isar, Technical University of Munich, Munich, Germany

Table 1 Scan parameters for MDCT protocol

Parameter	Value
Tube voltage (kVP)	120
Field of view (cm)	200
Beam collimation (mm)	0.625
Slice thickness (mm)	0.3
Helical pitch	0.758–0.914
$CTDI_{vol}$ (mGy)[a]	7.66 (2.3–13.7)
Tube current (mA)	200–400
Exposure (mAs)	112 (33–201)

[a]*$CTDI_{vol}$* volume computed tomography dose index

risk [5–8]; however, the applied radiation dose is currently not feasible for regular check-ups that require follow-up examinations [9]. Regular patient monitoring protocol for osteoporotic fracture risk cannot be established currently, because should multiple CT examinations be performed on the same patient, the effective radiation dosage could reach unsafe levels [10, 11].

Achieving an optimal diagnostic image quality and reduction in dose concurrently is the main goal of clinicians and researchers. There are currently several dose-reduction studies focusing on modification of reconstruction methods through iterative reconstruction algorithms [12–14]. Furthermore, dose reduction by means of modification of tube current modulation, reduction in tube potential, and scan time or length can also be performed [5, 11, 15, 16]. Therefore, the purpose of this study was (1) to evaluate whether MDCT with virtually reduced tube current, at half, quarter and tenth doses, compared to standard clinical dose, can be useful for predicting vertebral bone strength, as determined by FE analysis and (2) to assess whether the low-dose imaging can still be used to reliably differentiate patients with and without osteoporotic vertebral fractures.

Material and Methods

Study Population

This retrospective study was approved by the Institutional Review Board. Patients with vertebral fractures ($n=8$; 4 males and 4 females) were identified from routine thoracic and abdominal MDCT. There were 4 subjects with 1 fracture, 3 subjects with 2 fractures and 1 subject with 3 fractures. Age and gender-matched patients without osteoporotic fractures ($n=8$; 4 males and 4 females) were also identified as controls.

MDCT Imaging

All MDCT examinations were performed using a 256-row scanner (iCT, Philips Healthcare, Best, The Netherlands). A reference phantom (Mindways Osteoporosis Phantom, Austin, TX, USA) was placed beneath the scanner mat for all subjects. The scan parameters applied for the MDCT protocol are shown in Table 1. The tube voltage was kept constant at 120 kVp. The helical pitch was set as 0.758 for 1 subject, 0.79 for 1 subject and 0.954 for the remaining 14 subjects. The tube current ranged between 200 and 400 mA during each scan as it was modulated implicitly by the scanner. The exposure recorded for the subjects varied from 33 to 201 mAs for all 16 subjects. The volume CT dose index ($CTDI_{vol}$) ranged from 2.3 to 13.6 mGy. The variations are attributed to the different clinical purposes of the actual studies, since the subjects were not explicitly recruited for this study.

Tube Current Simulation

A simulation tool was used to generate lower tube current scans. The simulation algorithm was based on raw projection data, as described previously [17]. System parameters of the CT scanner were taken into account for electronic noise. Low-dose simulations at 50%, 25% and 10% of the original tube current were generated as reported previously [18]. Images were reconstructed using standard filtered back projection.

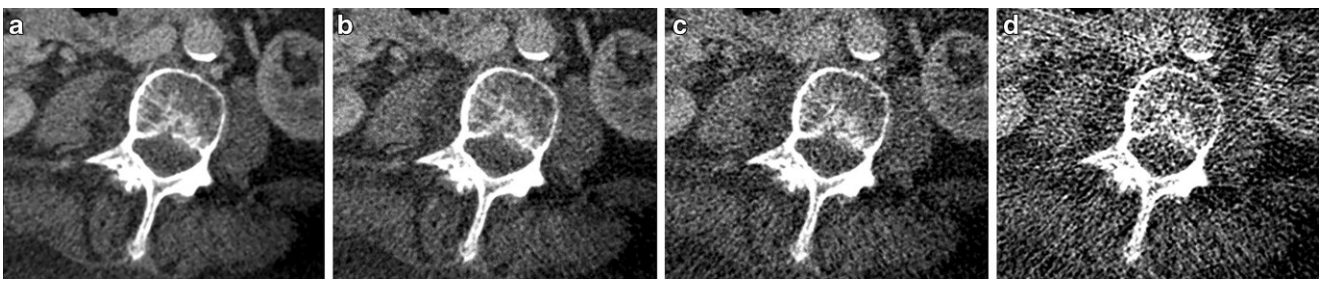

Fig. 1 MDCT images illustrating changes in image quality with dose reduction from standard (**a**) to half (**b**) to quarter (**c**) to tenth dose (**d**)

Table 2 Quantitative image analysis, reported as means and standard deviations, comparing fracture and control groups for all doses

Parameter	Standard dose		Half dose		Quarter dose		Tenth dose	
	Fracture	Control	Fracture	Control	Fracture	Control	Fracture	Control
Image noise (HU)	30.56 ± 4.90	35.55 ± 7.13	40.51 ± 4.94	55.59 ± 26.74	57.76 ± 7.85	64.58 ± 7.20	130.07 ± 33.89	158.38 ± 40.16
SNR	4.34 ± 1.56	4.88 ± 1.34	3.22 ± 0.93	3.41 ± 1.14	2.38 ± 0.72	2.79 ± 0.56	1.31 ± 0.58	1.28 ± 0.32
CNR	7.59 ± 2.16	7.78 ± 1.98	5.61 ± 1.35	5.63 ± 1.88	4.06 ± 1.04	4.64 ± 1.62	2.02 ± 0.82	1.95 ± 0.76

HU Hounsfield units, *SNR* signal-to-noise ratio, *CNR* contrast-to-noise ratio

Table 3 FE-predicted failure load values, reported as means and standard deviations, for fracture and control groups

	Fracture	Control	*p*-value
Standard dose	3254 ± 909	3794 ± 984	0.0373[a]
Half dose	3390 ± 890	3860 ± 1063	0.0305[a]
Quarter dose	3375 ± 915	3925 ± 990	0.0233[a]
Tenth dose	4513 ± 1762	4766 ± 1628	0.458
p-value (standard vs. half)	0.718	0.670	–
p-value (standard vs. quarter)	0.606	0.592	–
p-value (standard vs. tenth)	0.00198[a]	0.0354[a]	–

[a]Significant results

Image Segmentation

Manual segmentation of lumbar vertebrae (L1–3) was performed by one operator using the free open-source software MITK (German Cancer Research Center, Division of Medical and Biological Informatics, Medical Imaging Interaction Toolkit, Heidelberg, Germany). Fractured vertebrae were not observed at the L1–3 level.

Quantitative Image Analysis

Image parameters such as image noise, contrast-to-noise ratio (CNR) and signal-to-noise ratio (SNR) were measured by placing regions of interest (ROIs) on three slices; the mid-slice of the vertebra, the upper slice, 1 cm above the mid-slice and the lower slice, 1 cm below the mid-slice to minimize bias from single measurements. Hounsfield unit (HU) values measured over the three sequential slices were averaged to obtain signal and noise attenuations [19].

Finite Element Analysis

Numerical analysis was done on the simplistic assumption of an axial compression loading condition on each vertebra for all subjects. Image segmentation of each vertebra was imported into an image processing software Mimics (Materialise NV, Harislee, Belgium) and meshed with linear tetrahedral elements using a meshing software 3-Matic (Materialise NV). Each vertebral model was discretized into 10 different sets of heterogeneous, non-linear, transversely isotropic materials, based on a set of relationships provided in the literature for density, elastic modulus and strength [20–25]. A Poisson ratio of 0.3 was assumed and negative modulus regions were applied with 0.0001 MPa [26]. The FE analysis was performed with ABAQUS version 6.10 (Hibbitt, Karlsson, and Sorensen, Pawtucket, RI, USA). To simulate axial compression loading, nodes on the inferior endplate were constrained in all directions and a displacement load in the z-direction was applied on the nodes on the superior endplate [27]. Failure load was considered to be the peak of the force displacement curve obtained over the displacement increments. The FE method has also been described in previous studies [5, 6].

Statistical Analysis

Results were reported as means and standard deviations. To evaluate significant differences within each group, i. e. fracture and control, at different doses, with standard dose as the reference, Kruskal Wallis test was performed for quantitative image parameters and FE-predicted failure load values. To evaluate significant differences between the fracture and control groups at each dose, i. e. standard, half, quarter and tenth dose, Mann-Whitney test was performed. Correlations of the half, quarter and tenth doses, as a function of the standard doses were reported as Pearson's coefficient values (r) for both fracture and control groups. Bland-Altman plots, of each dose as a function of the standard dose were plotted, as it is useful for identifying a systematic bias between mean differences [28] and the respective Lin's concordance coefficients (r_c) were also reported. To evaluate the feasibility of low-dose to differentiate between fracture and control groups, receiver operating characteristic (ROC) curve analysis was performed and the area under the curve (AUC) was reported at each dose. All analyses were performed with MedCalc Statistical Software version 18 (MedCalc Software bvba, Ostend, Belgium; http://www.medcalc.org; 2018). Results obtained were considered to be significant at $p < 0.05$.

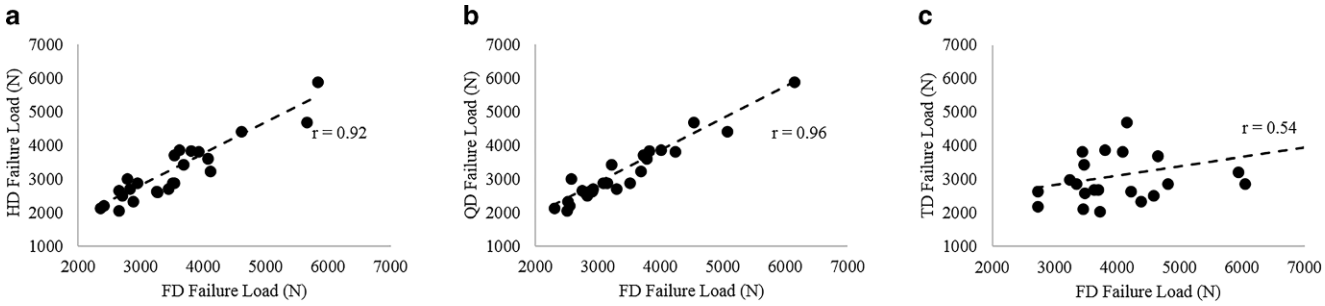

Fig. 2 Correlation between FE-predicted failure loads for each individual dose, half dose (*HD*) (**a**), quarter dose (*QD*) (**b**) and tenth dose (*TD*) (**c**) as a function of full dose (*FD*) for fracture group

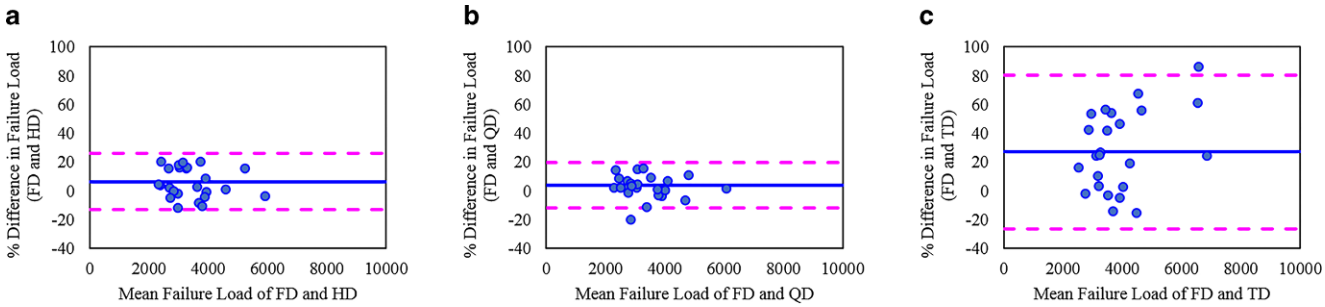

Fig. 3 Bland-Altman plots for each individual dose, half dose (*HD*) (**a**), quarter dose (*QD*) (**b**) and tenth dose (*TD*) (**c**) as a function of full dose (*FD*) for fracture group. The horizontal lines indicate the mean FE-predicted failure load, and 95% confidence intervals at ±1.96 standard deviation (*SD*)

Results

Quantitative Image Analysis

Changes in image quality by reduction of half, quarter and a tenth of a dose from standard dose are illustrated in Fig. 1. Means and standard deviations of noise, SNR and CNR are reported in Table 2. The mean image noise was 30.56, 40.51, 57.76, and 130.07 HU, mean SNR was 4.34, 3.22, 2.38 and 1.31 and mean CNR was 7.59, 5.61, 4.06 and 2.03 in the full, half, quarter, and tenth dose examinations, respectively for the fracture group. In the control group, the mean image noise was 35.55, 55.59, 64.58, 158.38 HU, mean SNR was 4.89, 3.41, 2.79 and 1.28 and mean CNR was 7.78, 5.63, 4.64, and 1.95, respectively. For the fracture and control groups the mean image noise, SNR, and CNR of standard dose were significantly different between the half, quarter, and tenth doses ($p < 0.05$).

Comparison of FE-Predicted Failure Loads

Table 3 provides the means and standard deviations for all doses for the fracture and control groups. In evaluating the differences between the individual doses and standard dose as the reference for the fracture and control groups, respectively, the failure load of the standard dose did not significantly differ from the half ($p = 0.718$ and $p = 0.670$) and quarter doses ($p = 0.606$ and $p = 0.592$); however, it significantly differed from the tenth dose ($p = 0.00198$ and $p = 0.0354$; Table 3). In evaluating the differences at each dose, the failure load differed significantly between fracture and control groups at standard ($p = 0.0373$), half ($p = 0.0305$), and quarter doses ($p = 0.0233$) but not at tenth dose ($p = 0.458$; Table 3).

In the fracture group, significant correlations were obtained with FE-predicted failure load values for half dose ($r = 0.92$, $p < 0.0001$), quarter dose ($r = 0.96$, $p < 0.0001$), and tenth dose ($r = 0.54$, $p = 0.0061$) with full dose as the reference (Fig. 2a–c). Amongst the control group, significant correlations were exhibited for half ($r = 0.97$, $p < 0.0001$), quarter ($r = 0.93$, $p < 0.0001$) and tenth ($r = 0.90$, $p < 0.0001$) doses with full dose as the reference (Fig. 3a–c). Bland-Altman plots showed that there was good concordance for half dose ($r_c = 0.94$) and quarter dose ($r_c = 0.95$) with the standard dose, but not for tenth dose ($r_c = 0.31$) in the fracture group (Fig. 4a–c). For the control group, there was good concordance for half dose ($r_c = 0.97$), quarter dose ($r_c = 0.92$) and tenth dose ($r_c = 0.62$; Fig. 5a–c).

The ROC curve analysis for the ability of the doses to be able to differentiate patients with and without fractures revealed the following: full dose was able to differentiate significantly (AUC = 0.675, $p = 0.0266$), as well as half dose (AUC = 0.686, $p = 0.0188$) and quarter dose (AUC = 0.691, $p = 0.0137$); however, the tenth dose was not able to dif-

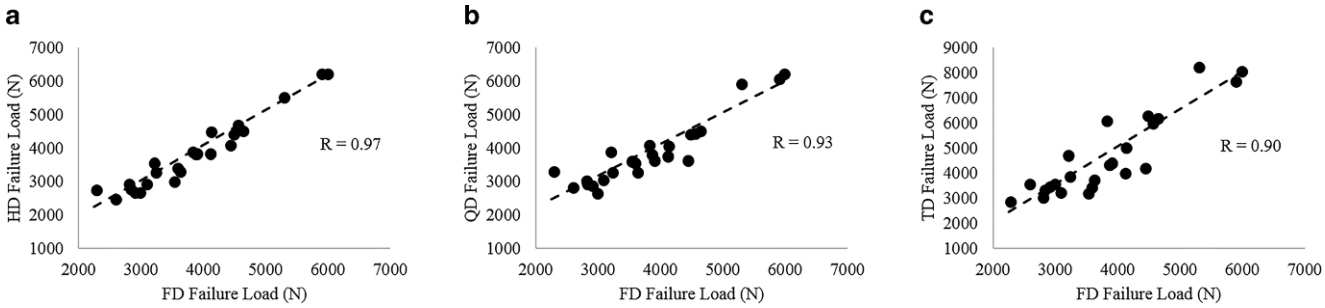

Fig. 4 Correlation between FE-predicted failure loads for each individual dose, half dose (*HD*) (**a**), quarter dose (*QD*) (**b**) and tenth dose (*TD*) (**c**) as a function of full dose (*FD*) for control group

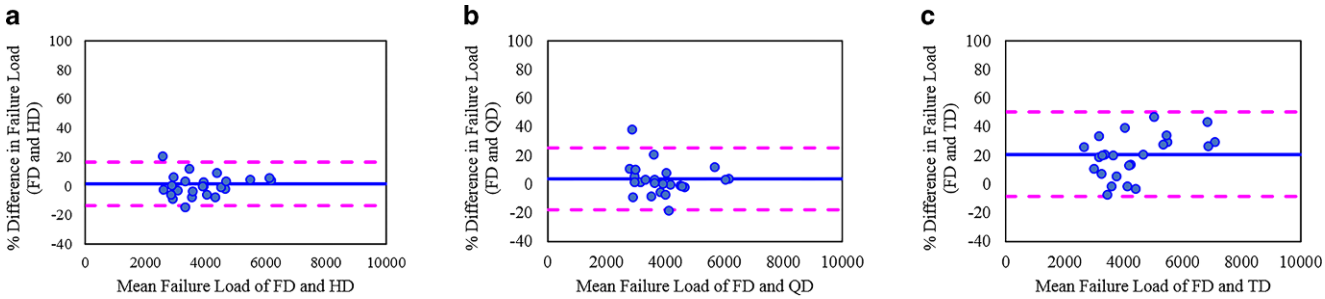

Fig. 5 Bland-Altman plots for each individual dose, half dose (*HD*) (**a**), quarter dose (*QD*) (**b**) and tenth dose (*TD*) (**c**) as a function of full dose (*FD*) for control group. The horizontal lines indicate the mean FE-predicted failure load, and 95% confidence intervals at ±1.96 standard deviation (*SD*)

ferentiate between the two patient groups (AUC = 0.562, $p = 0.461$). In the pairwise comparison of ROC curves, there were no significant differences between areas of the half and quarter doses, compared to the full dose.

Discussion

The need for low-dose CT examinations to evaluate the stability and integrity of the spine is of utmost importance in the orthopedic and neurosurgical scene. To our knowledge, this is the only study that has explored the possibility of non-invasive failure load prediction of patients with and without fractures using FE analysis at the ultra-low dose level.

With the reduction in dose, the image noise significantly increased in the half, quarter and tenth dose examinations, while SNR and CNR significantly worsened for both groups. Although the image noise increased by 33% and 56% at half dose and 89% and 82% at quarter dose for the fracture and control groups, respectively, the FE-predicted failure load obtained at half and quarter doses had minimal differences from the standard dose. This key finding demonstrates that MDCT images at half and quarter doses can produce accurate structural information; however, at the tenth dose, FE-predicted failure load only agreed well with the standard dose in the healthy group, and not in the fracture group. The reason for the difference could be attributed to the poor geometry of vertebra obtained from the fracture group, which is affected by the presence of spinal deformities as well as higher surface roughness as a result. Consequently, meshes with the presence of sharp boundaries can result in inaccurate failure load values; however, this phenomenon needs further investigation with future work involving large population cohorts.

The ROC analysis demonstrated that standard, half and quarter doses were able to successfully differentiate fracture from control groups with similar AUCs greater than 65%, except for the tenth dose, which was only 56%. This finding shows that FE analysis could be useful in providing non-invasive structural information, which would be valuable to clinicians, on top of obtaining the current gold standard, BMD for a more holistic understanding of fracture risk.

The establishment of an optimal imaging protocol is even more necessary than before, especially with radiology departments working with standard protocols. Dose optimization protocols could result in a 30% reduction in collective dosage produced by MDCT and this reduction can be sustained over time [29]. By reducing the radiation dose in each CT scan, much of the radiation exposure subjected to the patients can be avoided, particularly if they are undergoing annual or regular follow-up radiological examinations.

The main limitation of this study is that this is a retrospective study of a small sample. A larger population

cohort study will enable the results obtained in this study to be confirmed. Nevertheless, these results are promising as a pilot study in providing a possibility of a more holistic investigation of vertebral fracture risk in osteoporotic patients. Beyond low-dose MDCT-based FEM, alternative approaches for fracture risk prediction, e. g. based on projection radiography or EOS imaging, may also be options in the future. In addition, future work will also include FE analysis based on different kernels with FBP and iterative reconstruction algorithms, which have the potential to produce better quality images at low radiation doses.

In conclusion, low-dose MDCT up to a 75% dose reduction has been shown to be a reliable method to assess FE-predicted failure load in the vertebra. Although in its early phases of realization, MDCT dose reduction techniques and the combined use of non-invasive FE analysis are expected to act as a complementary tool to BMD for assessing fracture risk in the future, which has great potential to benefit patients with osteoporosis.

Funding This study received funding by the Deutsche Forschungsgemeinschaft (DFG) BA 4906/2-1 (TB), and TUM Faculty of Medicine KKF grant H01 (TB).

Conflict of interest D. Anitha, K. Mei, M. Dieckmeyer, F.K. Kopp, N. Sollmann, C. Zimmer, J.S. Kirschke, P.B. Noel, T. Baum and K. Subburaj declare that they have no competing interests.

References

1. Francis RM, Aspray TJ, Hide G, Sutcliffe AM, Wilkinson P. Back pain in osteoporotic vertebral fractures. Osteoporos Int. 2008;19:895–903.
2. Schuit SC, van der Klift M, Weel AE, de Laet CE, Burger H, Seeman E, Hofman A, Uitterlinden AG, van Leeuwen JP, Pols HA. Fracture incidence and association with bone mineral density in elderly men and women: the Rotterdam Study. Bone. 2004;34:195–202.
3. Wang X, Sanyal A, Cawthon PM, Palermo L, Jekir M, Christensen J, Ensrud KE, Cummings SR, Orwoll E, Black DM; Osteoporotic Fractures in Men (MrOS) Research Group, Keaveny TM. Prediction of new clinical vertebral fractures in elderly men using finite element analysis of CT scans. J Bone Miner Res. 2012;27:808–16.
4. Kopperdahl DL, Aspelund T, Hoffmann PF, Sigurdsson S, Siggeirsdottir K, Harris TB, Gudnason V, Keaveny TM. Assessment of incident spine and hip fractures in women and men using finite element analysis of CT scans. J Bone Miner Res. 2014;29:570–80.
5. Anitha D, Subburaj K, Mei K, Kopp FK, Foehr P, Noel PB, Kirschke JS, Baum T. Effects of dose reduction on bone strength prediction using finite element analysis. Sci Rep. 2016;6:38441.
6. Anitha D, Subburaj K, Baum T, Kirschke JS. Vertebral stability in multiple myeloma patients: a finite-element study. European Orthopaedic Research Society 24th Annual Meeting; Bologna, Italy. 2016.
7. Bauer JS, Sidorenko I, Mueller D, Baum T, Issever AS, Eckstein F, Rummeny EJ, Link TM, Raeth CW. Prediction of bone strength by muCT and MDCT-based finite-element-models: how much spatial resolution is needed? Eur J Radiol. 2014;83:e36–42.
8. Liebl H, Garcia EG, Holzner F, Noel PB, Burgkart R, Rummeny EJ, Baum T, Bauer JS. In-vivo assessment of femoral bone strength using Finite Element Analysis (FEA) based on routine MDCT imaging: a preliminary study on patients with vertebral fractures. PLoS One. 2015;10:e116907.
9. Yi JW, Park HJ, Lee SY, Rho MH, Hong HP, Choi YJ, Kim MS. Radiation dose reduction in multidetector CT in fracture evaluation. Br J Radiol. 2017;90(1077):20170240.
10. Wiest PW, Locken JA, Heintz PH, Mettler FA Jr.. CT scanning: a major source of radiation exposure. Semin Ultrasound Ct Mr. 2002;23:402–10.
11. Costello JE, Cecava ND, Tucker JE, Bau JL. CT radiation dose: current controversies and dose reduction strategies. AJR Am J Roentgenol. 2013;201:1283–90.
12. Pontana F, Duhamel A, Pagniez J, Flohr T, Faivre JB, Hachulla AL, Remy J, Remy-Jardin M. Chest computed tomography using iterative reconstruction vs filtered back projection (Part 2): image quality of low-dose CT examinations in 80 patients. Eur Radiol. 2011;21:636–43.
13. Niu YT, Mehta D, Zhang ZR, Zhang YX, Liu YF, Kang TL, Xian JF, Wang ZC. Radiation dose reduction in temporal bone CT with iterative reconstruction technique. AJNR Am J Neuroradiol. 2012;33:1020–6.
14. Silva AC, Lawder HJ, Hara A, Kujak J, Pavlicek W. Innovations in CT dose reduction strategy: application of the adaptive statistical iterative reconstruction algorithm. AJR Am J Roentgenol. 2010;194:191–9.
15. Konda SR, Goch AM, Leucht P, Christiano A, Gyftopoulos S, Yoeli G, Egol KA. The use of ultra-low-dose CT scans for the evaluation of limb fractures. Bone Jt J. 2016;98-B:1668–73.
16. Mulkens TH, Marchal P, Daineffe S, Salgado R, Bellinck P, te Rijdt B, Kegelaers B, Termote JL. Comparison of low-dose with standard-dose multidetector CT in cervical spine trauma. AJNR Am J Neuroradiol. 2007;28:1444–50.
17. Zabić S, Wang Q, Morton T, Brown KM. A low dose simulation tool for CT systems with energy integrating detectors. Med Phys. 2013;40:31102.
18. Mei K, Kopp FK, Bippus R, Köhler T, Schwaiger BJ, Gersing AS, Fehringer A, Sauter A, Münzel D, Pfeiffer F, Rummeny EJ, Kirschke JS, Noël PB, Baum T. Is multidetector CT-based bone mineral density and quantitative bone microstructure assessment at the spine still feasible using ultra-low tube current and sparse sampling? Eur Radiol. 2017;27:5261–71.
19. Huber MB, Carballido-Gamio J, Bauer JS, Baum T, Eckstein F, Lochmüller EM, Majumdar S, Link TM. Proximal femur specimens: Automated 3D trabecular bone mineral density analysis at multidetector CT—Correlation with biomechanical strength measurement. Radiology. 2008;247:472–81.
20. Rho JY, Hobatho MC, Ashman RB. Relations of mechanical properties to density and CT numbers in human bone. Med Eng Phys. 1995;17:347–55.
21. Goulet RW, Goldstein SA, Ciarelli MJ, Kuhn JL, Brown MB, Feldkamp LA. The relationship between the structural and orthogonal compressive properties of trabecular bone. J Biomech. 1994;27:375–89.
22. Keller TS. Predicting the compressive mechanical behavior of bone. J Biomech. 1994;27:1159–68.
23. Keyak JH. Improved prediction of proximal femoral fracture load using nonlinear finite element models. Med Eng Phys. 2001;23:165–73.
24. Keyak JH, Lee IY, Skinner HB. Correlations between orthogonal mechanical-properties and density of trabecular bone—use of different densitometric measures. J Biomed Mater Res. 1994;28:1329–36.
25. Keyak JH, Falkinstein Y. Comparison of in situ and in vitro CT scan-based finite element model predictions of proximal femoral fracture load. Med Eng Phys. 2003;25:781–7.

26. Crawford RP, Cann CE, Keaveny TM. Finite element models predict in vitro vertebral body compressive strength better than quantitative computed tomography. Bone. 2003;33:744–50.
27. Imai K. Analysis of vertebral bone strength, fracture pattern, and fracture location: a validation study using a computed tomography-based nonlinear finite element analysis. Aging Dis. 2015;6:180–7.
28. Giavarina D. Understanding Bland Altman analysis. Biochem Med (Zagreb). 2015;25:141–51.
29. Tack D, Jahnen A, Kohler S, Harpes N, De Maertelaer V, Back C, Gevenois PA. Multidetector CT radiation dose optimisation in adults: short- and long-term effects of a clinical audit. Eur Radiol. 2014;24:169–75.